LHCb-CONF-2012-011
April 4, 2012

Measurement of the cross-section for $Z^0 \to e^+e^-$ production in pp collisions at $\sqrt{s} = 7$ TeV

The LHCb collaboration [†]

Abstract

A measurement of the cross-section for $Z^0 \to e^+e^-$ at $\sqrt{s} = 7$ TeV is presented using LHCb data recorded in 2011 corresponding to an integrated luminosity of $945\,\text{pb}^{-1}$. Within the kinematic acceptance, $p_T > 20$ GeV and $2 < \eta < 4.5$ for the leptons and $60 < M < 120$ GeV and $2 < y < 4$ for the Z^0, the cross-section is measured to be

$$\sigma(Z^0 \to e^+e^-) = 75.7 \pm 0.5(\text{stat.}) \pm 2.4(\text{syst.}) \pm 2.6(\text{lumi.})\ \text{pb}\ .$$

The results are compared with previous measurements and with theoretical predictions using QCD at NNLO.

[†]Conference report prepared for XX International Workshop on Deep Inelastic Scattering and Related Subjects (Bonn, March 2012); contact author: David Ward, drw1@cam.ac.uk.

1 Introduction

The measurement of vector boson production in LHCb permits a number of tests of electroweak physics and of QCD. In particular, the kinematic range of LHCb, roughly $2 < \eta < 5$[1], complements that of the general purpose detectors ATLAS and CMS. Measurements at LHCb are sensitive to knowledge of the proton structure functions at very low Bjorken x values, at which the parton distribution functions (PDFs) are not particularly well constrained by previous data from HERA, see for example Ref. [1].

The most straightforward decay modes for LHCb to study the $W^{\pm}$ and Z^0 bosons are the muonic channels, $Z^0 \to \mu^+\mu^-$ and $W^+ \to \mu^+\nu_\mu$, since a highly efficient trigger for high momentum muons exists. However, it is desirable to examine also the electron channels $Z^0 \to e^+e^-$ and $W^+ \to e^+\nu_e$, which offer statistically independent samples, with different systematic uncertainties.

The main difficulty with electron reconstruction in LHCb is the energy measurement. A significant amount of material is traversed by the particles before they reach the momentum analysing magnet, and their energies are therefore liable to be degraded by bremsstrahlung. For low energy electrons, the bremsstrahlung photons can frequently be identified in the electromagnetic calorimeter, and added in to the measured energy of the electron. However, in the case of $W^{\pm}$ and Z^0 decays, the electrons are of high momentum and $p_{\rm T}$, so that the bremsstrahlung photons are not generally separated from the electrons. Furthermore, because the energies recorded in individual calorimeter cells saturate at $E_{\rm T} \sim 10$ GeV, it is not possible to substitute the calorimeter energy for the momentum measured using the spectrometer. We therefore have to deal with a situation in which the electron directions are well determined, but their energies are degraded by a variable amount, typically $\sim 25\%$.

In this note, we present a measurement of the cross-section for $Z^0 \to e^+e^-$ using the data recorded by LHCb in 2011. For ease of comparison, the measurement is performed in the same kinematic region as the recent measurement of $Z^0 \to \mu^+\mu^-$ in the 2010 data [2, 3], $60 < M < 120$ GeV and $2 < y < 4$ for the Z^0, and $2 < \eta < 4.5$ and $p_{\rm T} > 20$ GeV for the lepton[2]. As the rapidity of the Z^0 can be well determined, to a precision of ~ 0.05, the rapidity distribution will be presented. However, the $p_{\rm T}$ of the Z^0 is poorly determined, and its distribution will not be discussed here. After a brief description of the detector, Sect. 3 then describes the event selection, and Sect. 4 outlines the techniques used for determining the various efficiencies for event detection. The results are laid out in Sect. 5 followed by a brief summary.

[1] In this paper, y denotes rapidity, η pseudorapidity, M mass, $p_{\rm T}$ transverse momentum and $E_{\rm T}$ transverse energy.

[2] Natural units in which $c = 1$ are used throughout.

2 LHCb detector

The LHCb detector [4] is a single-arm forward spectrometer covering the pseudorapidity range $2 < \eta < 5$, designed for the study of particles containing b or c quarks. The detector includes a high precision tracking system consisting of a silicon-strip vertex detector surrounding the pp interaction region, a large-area silicon-strip detector located upstream of a dipole magnet with a bending power of about 4 Tm, and three stations of silicon-strip detectors and straw drift tubes placed downstream. The combined tracking system has a momentum resolution $\Delta p/p$ that varies from 0.4% at 5 GeV/c to 0.6% at 100 GeV/c, and an impact parameter resolution of 20 μm for tracks with high transverse momentum. Charged hadrons are identified using two ring-imaging Cherenkov detectors. Photon, electron and hadron candidates are identified by a calorimeter system consisting of scintillating-pad (SPD) and preshower (PRS) detectors, an electromagnetic calorimeter (ECAL) and a hadronic calorimeter (HCAL). Muons are identified by a muon system composed of alternating layers of iron and multiwire proportional chambers. The trigger consists of a hardware stage, based on information from the calorimeter and muon systems, followed by a software stage which applies a full event reconstruction.

The data selection used for the present analysis includes a requirement that events were triggered through specified single-electron trigger lines. Furthermore, the trigger was required to have been activated at each stage by at least one of the electrons forming the Z^0 candidate. One significant improvement to the relevant trigger lines occurred during August 2011, affecting the trigger efficiency. The data samples before and after this change were treated separately, and will be referred to as Data Sample I and Data Sample II. These were found to correspond to integrated luminosities of 581.4 ± 20.3 pb^{-1} and 363.5 ± 12.7 pb^{-1} respectively, or a total of 944.9 ± 33.1 pb^{-1}.

3 Event selection

The $Z^0 \to e^+e^-$ selection starts from a sample of e^+e^- candidates having high invariant mass. The analysis cuts are as follows:

- Triggers selecting a single high E_T electron should have been satisfied by at least one of the electrons in the candidate, at each of the stages of the trigger. The relevant triggers demand an electron having $E_T > 10 - 15$ GeV.
- Cuts are imposed to achieve good track quality. The χ^2 of the track fit should satisfy $\chi^2/\text{dof} < 5$ and a requirement on the momentum error, $\Delta p/p < 0.1$, is used to remove tracks with poorly measured momentum or charge.
- The electrons are both required to have measured $p_T > 20$ GeV and pseudorapidities in the range $2.0 < \eta < 4.5$. The pseudorapidity cut reflects the detector acceptance, and the p_T cut serves to remove most forms of background.
- The invariant mass of the e^+e^- pair should be greater than 40 GeV.

- Particle identification (PID): the following cuts on calorimeter information are used to provide electron identification:
  - $E_{\rm ECAL}/p > 0.1$, where p is the track momentum, with bremsstrahlung correction if available, and $E_{\rm ECAL}$ is the ECAL energy associated with the particle;
  - $E_{\rm HCAL}/p < 0.05$, where $E_{\rm HCAL}$ is the HCAL energy associated with the particle;
  - $E_{\rm PRS} > 50$ MeV, where $E_{\rm PRS}$ is the energy in the preshower detector associated with the particle.

  These cuts essentially impose an electromagnetic shower profile, while being loose enough not to lose many genuine electrons, despite the effects of calorimeter saturation and bremsstrahlung.

A second sample of same-sign $e^{\pm}e^{\pm}$ combinations, subject to the same selection criteria, is used to provide a data-based estimate of background. We would expect the main contribution to background to arise from hadrons which happen to shower early in the ECAL, and consequently fake the shower signature of an electron. It seems reasonable to expect these to contribute equally to same-sign and opposite-sign pairs. The contribution from semileptonic heavy flavour decays should be similar to that in the $Z^0 \to \mu^+\mu^-$ channel, which was found to be very small [2, 3]; in any case, subtracting the same-sign contribution should account for most of this effect. The contribution arising from electrons produced from pion or kaon decays will be greatly suppressed compared to the muon channel because $\pi^{\pm}$ and $K^{\pm}$ have much lower branching ratios to electrons than to muons.

Simulated event samples of $Z^0/\gamma^* \to e^+e^-$ (with $M(e^+e^-) > 40$ GeV) are also used to assess some efficiencies, and simulated samples of $Z^0 \to \tau^+\tau^-$ and of $t\bar{t}$ are used to determine possible background contributions. These samples were generated using Pythia version 6.4 [5] configured as described in Ref. [6] and using the CTEQ6L1 PDF set [7], and were then processed through a Geant4 [8] application [9] which simulates the LHCb detector. The simulated events are then reconstructed as for data, including simulation of the trigger.

The invariant mass distribution of the selected candidates is shown in Fig. 1. The distribution falls off abruptly above the Z^0 mass, which is strong confirmation that the $Z^0 \to e^+e^-$ decay is seen, and is spread to lower masses by the effect of bremsstrahlung. The shape is further moulded by the kinematic cuts. The agreement in shape between data and simulation is good; this will be further discussed below. The background as estimated from same-sign events amounts to 2.2%, and that from $\tau^+\tau^-$ events is estimated to be a negligible 0.1%. Possible background from $t\bar{t}$ events is estimated to be below the 0.1% level.

Further checks on the kinematic properties of the selected events indicate that the data are in good agreement with the expectations from simulation, providing some reassurance that the simulated events can be used in the correction procedure if necessary. However, whenever possible, corrections are estimated from the data themselves.

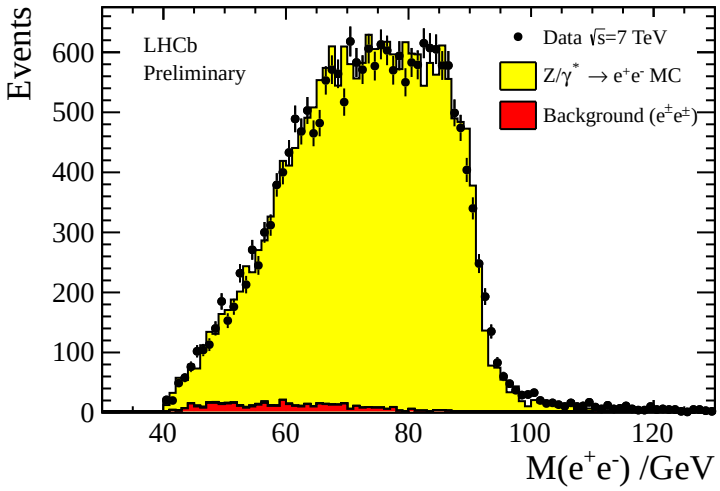

Figure 1: Invariant mass distribution of $Z^0 \to e^+e^-$ candidates. The data are shown as points with errors, the background obtained from same-sign data is shown in red, to which the expectation from signal simulation is added in yellow. The $\tau^+\tau^-$ contribution is also included (though not visible), and the Monte Carlo has been normalised to the (background-subtracted) data.

4 Correction of the data

The determination of the cross-section is based on the formula

$$\sigma = \frac{N(e^+e^-) - N(e^\pm e^\pm)}{\epsilon_{\rm GEC} \cdot \epsilon_{\rm trig} \cdot \epsilon_{\rm track} \cdot \epsilon_{\rm kin} \cdot \epsilon_{\rm PID} \cdot \int \mathcal{L} dt} \cdot f_{\rm FSR} \cdot f_{\rm MZ} \quad , \tag{1}$$

where $N(e^+e^-)$ is the number of Z^0 candidates selected in data, $N(e^\pm e^\pm)$ the background estimated from the number of same-sign candidates and $\int \mathcal{L} dt$ is the integrated luminosity. The meaning and estimation of the five efficiency factors (ϵ) are explained in the following sections, and $f_{\rm FSR}$ is a correction factor for final-state electromagnetic radiation, thus correcting the measurement to the Born level. Finally, the factor $f_{\rm MZ}$ corrects for $Z^0/\gamma^* \to e^+e^-$ events whose true mass lies outside the range $60 < M < 120$ GeV and which pass the event selection. The correction procedure is applied for four separate equal-width bins in Z^0 rapidity in the range $2 < y < 4$.

The luminosity was determined as described in Ref. [10], and has an associated error of 3.5%. The final-state radiative correction, $f_{\rm FSR}$ is obtained by the same procedure as for the $\mu^+\mu^-$ channel [2] – using PHOTOS [11] interfaced to PYTHIA [5], with the HORACE [12] generator used as a cross-check. This correction is approximately twice as large for the e^+e^- final state as for the $\mu^+\mu^-$ final state.

The measured cross-section is intended to refer to the kinematic range $60 < M < 120$ GeV (for comparison with the $Z^0 \to \mu^+\mu^-$ results). The selected sample has a lower cut on measured mass, $M(e^+e^-) > 40$ GeV, in order to accept more events with bremsstrahlung. However, there is some small chance that Drell-Yan events with true

Table 1: Efficiencies and other factors needed for the cross-section determination, in bins of the Z^0 rapidity, y. The two data samples recorded before (I) and after (II) August 2011, when the electron trigger was changed, are treated separately.

	$2 < y < 2.5$	$2.5 < y < 3$	$3 < y < 3.5$	$3.5 < y < 4$
$\epsilon_{\rm GEC}$	0.950 ± 0.010			
$\epsilon_{\rm trig}$ (I)	0.680 ± 0.039	0.672 ± 0.027	0.701 ± 0.033	0.557 ± 0.081
$\epsilon_{\rm trig}$ (II)	0.883 ± 0.006	0.887 ± 0.004	0.907 ± 0.004	0.911 ± 0.011
$\epsilon_{\rm track}$	0.923 ± 0.015	0.925 ± 0.014	0.892 ± 0.015	0.863 ± 0.015
$\epsilon_{\rm kin}$	0.558 ± 0.010	0.528 ± 0.011	0.446 ± 0.013	0.386 ± 0.018
$\epsilon_{\rm PID}$	0.897 ± 0.007	0.927 ± 0.005	0.935 ± 0.008	0.848 ± 0.024
$f_{\rm FSR}$	1.042 ± 0.001	1.049 ± 0.001	1.053 ± 0.001	1.053 ± 0.002
$f_{\rm MZ}$	0.968 ± 0.001	0.974 ± 0.001	0.972 ± 0.001	0.935 ± 0.004
$\int \mathcal{L}dt$ / pb^{-1} (I)	581.4 ± 20.3			
$\int \mathcal{L}dt$ / pb^{-1} (II)	363.5 ± 12.7			
Sel. e^+e^- events (I)	2257	5445	3720	603
Sel. $e^\pm e^\pm$ events (I)	38	111	75	25
Sel. e^+e^- events (II)	1814	4256	2977	454
Sel. $e^\pm e^\pm$ events (II)	39	76	96	18

mass outside the $60 < M < 120$ GeV range will be selected, and this is corrected by the factor $f_{\rm MZ}$ — evaluated from Monte Carlo by examining the true Z^0/γ^* mass for selected events. The values obtained for the efficiencies and other factors are summarised in Table 1.

4.1 Global event cuts

Global event cuts (GEC) are applied in the triggering in order to prevent very large events from dominating the processing time. In the $Z^0 \to e^+e^-$ case, the critical cut is that the multiplicity of SPD hits be $N_{\rm SPD} \leq 600$. The impact of this cut is strongly dependent on the number of primary vertices reconstructed in the event. The inefficiency introduced by this cut is assessed by comparing with the $Z^0 \to \mu^+\mu^-$ case, for which a less stringent cut of 900 hits was imposed for events passing the dimuon trigger. The loss of $Z^0 \to e^+e^-$ events in the range $600 < N_{\rm SPD} \leq 900$ can be assessed by counting the events in the $\mu^+\mu^-$ distribution between 600 and 900 SPD hits. The contribution above 900 is very small ($\sim 0.2\%$ overall), and is estimated by fitting a Γ-function to the $\mu^+\mu^-$ distribution and using it to extrapolate. This procedure is adopted for each number of reconstructed primary vertices, and the results combined to obtain the overall efficiency, $\epsilon_{\rm GEC} = 0.950 \pm 0.010$, where the uncertainty is estimated by making reasonable changes to the procedure. This efficiency is not found to depend significantly on y, so the same value is used for all bins of Z^0 rapidity.

4.2 Trigger efficiencies

The trigger efficiencies for events passing the final selection cuts are determined from the data. The procedure is validated on simulated events, for which the true efficiency can also be determined, and is found to give correct results within the statistical errors. The principle is to identify a sample of events which are triggered independently of the positron (for example), and to use it to determine the efficiency for triggering the positron, and likewise for the electron. For example, denoting the total numbers of candidates for which the single electron trigger was satisfied at each stage by the electron N^-, by the positron N^+ and by both N^{+-}, the efficiency for triggering the electron is given by $\varepsilon^- = N^{+-}/N^+$, and likewise for the positron. The overall efficiency is then taken to be $\varepsilon^- + \varepsilon^+ - \varepsilon^-\varepsilon^+$, assuming that the positron and electron are triggered independently, an assumption which is validated by the test on simulated samples. The determination is performed separately in each bin of Z^0 rapidity. However, for Data Sample I an unwanted feature of the trigger software means that a variant of this procedure is needed, which leads to a less precise efficiency determination. In all cases, the statistical uncertainty on the efficiency determination is taken as a contribution towards the systematic error on the measurement.

4.3 Track-finding efficiency

The track-finding efficiency represents the probability that both of the electrons are successfully reconstructed as tracks which pass the track quality cuts. It is estimated, in bins of Z^0 rapidity, using Monte Carlo simulation by determining the probability that in a true $Z^0 \to e^+e^-$ event within the kinematic acceptance, both of the electrons are associated with reconstructed tracks satisfying the track quality cuts (but not necessarily the kinematic cuts). Its statistical precision is treated as a contribution to the systematic error. We also include a systematic uncertainty based on data-driven estimates made for muons from J/ψ decays.

4.4 Kinematic efficiency

The kinematic efficiency represents the probability that, in a true $Z^0 \to e^+e^-$ event within the kinematic acceptance in which both electrons are reconstructed, the tracks pass the kinematic selection cuts $2 < \eta < 4.5$ and $p_T > 20$ GeV. This is a sizeable correction, because of bremsstrahlung, which leads to a significant fraction of particles with true $p_T > 20$ GeV having reconstructed $p_T < 20$ GeV. The efficiency is estimated from simulation, with its statistical precision being treated as a contribution to the systematic uncertainty.

This determination relies on a faithful description of the material in the simulation program, which can be tested using data. For example, if the amount of material was underestimated, the reconstructed electron momenta would be shifted to lower values on average. This would be seen as a shift in, for example, the reconstructed mass spectrum shown in Fig. 1. By comparing the shape of the reconstructed mass spectrum and other kinematic distributions in data and simulation samples, we assign a systematic error on

the momentum scale and hence on the kinematic efficiency. This is combined with the statistical uncertainty mentioned above.

4.5 PID efficiency

The PID efficiency represents the probability that a reconstructed electron track, satisfying the kinematic requirements, also satisfies the calorimeter energy cuts used to identify electrons. This includes the probability that the track is within the calorimeter acceptance and has been successfully associated with calorimeter information. The PID efficiency can be estimated directly from data, rather than relying on simulation.

Starting from a sample which requires just one high p_{T} electron, events are selected by applying the usual criteria, except that only one of the e^+ and e^- (the "tag") is required to pass the calorimeter-based electron identification cuts. The other track is used as a "probe" to test the PID efficiency. The requirement on only one identified electron admits a significant level of background, which is assessed by examining the p_{T} distribution of the tag electron. This distribution of the tag electrons displays a clear shoulder extending to ~ 45 GeV above a falling background (arising from the usual Jacobian peak, modified by the effect of bremsstrahlung); the size of this contribution can be used to define the number of Z^0 events which fail the PID, and hence to determine the PID efficiency and its error for a single electron. The square of this efficiency is used as ϵ_{PID}.

5 Results

Using Eq. 1 and the information detailed in Table 1 we obtain the cross-section measurements listed in Table 2. The total cross-sections integrated over the range $2 < y < 4$ are obtained by summing the individual bins, taking the errors associated with the GEC efficiency, the kinematic efficiency and the luminosity to be fully correlated between bins, and the other contributions to be uncorrelated. We note that the results for the two data samples are consistent, despite their significantly different trigger efficiencies, which provides some confidence in the approach taken in their derivation. The results from the two data samples are then combined, assuming their errors to be fully correlated apart from the statistical error and the uncertainty in the trigger efficiency. The second period has lower integrated luminosity, but higher and more accurately estimated trigger efficiency. The choice made is to give the two samples equal weight in the combination – this comes close to yielding the smallest overall error. The final measurement of the cross-section has a total relative error of 4.5%, dominated by the 3.5% luminosity uncertainty. The statistical error is 0.7% and the total experimental systematic 2.8%.

Since the results have been corrected using the factor f_{FSR} to the Born level, it is possible to compare them with the same theoretical calculations used in the $\mathrm{Z}^0 \to \mu^+\mu^-$ analysis [2]. These calculations are performed at NNLO in QCD using the program DYNNLO [13]. With this, the NNLO PDF sets of MSTW08 [14], ABKM09 [15], JR09 [16], HERA15 [17] and NNPDF21 [18] are used along with the NLO set CTEQ6M [7]. The

Table 2: Measurements of the $Z^0 \to e^+e^-$ production cross-section at 7 TeV as a function of the Z^0 rapidity, y. The first error is the statistical uncertainty, the second is the experimental systematic uncertainty, and the third is the luminosity uncertainty. The error on the FSR correction is negligible. The results are given for the two separate data samples discussed above, and for the full sample combined.

y	Data sample I /pb	Data sample II /pb	Combined /pb
2.0—2.5	$12.9 \pm 0.3 \pm 0.8 \pm 0.5$	$12.7 \pm 0.3 \pm 0.4 \pm 0.4$	$12.8 \pm 0.2 \pm 0.5 \pm 0.4$
2.5—3.0	$32.4 \pm 0.5 \pm 1.6 \pm 1.1$	$30.8 \pm 0.5 \pm 0.9 \pm 1.1$	$31.6 \pm 0.3 \pm 1.1 \pm 1.1$
3.0—3.5	$25.9 \pm 0.4 \pm 1.5 \pm 0.9$	$25.3 \pm 0.5 \pm 0.9 \pm 0.9$	$25.6 \pm 0.3 \pm 1.1 \pm 0.9$
3.5—4.0	$6.5 \pm 0.3 \pm 1.0 \pm 0.2$	$4.8 \pm 0.2 \pm 0.3 \pm 0.2$	$5.7 \pm 0.2 \pm 0.5 \pm 0.2$
Sum	$77.8 \pm 0.7 \pm 3.1 \pm 2.7$	$73.6 \pm 0.8 \pm 2.1 \pm 2.6$	$75.7 \pm 0.5 \pm 2.4 \pm 2.6$

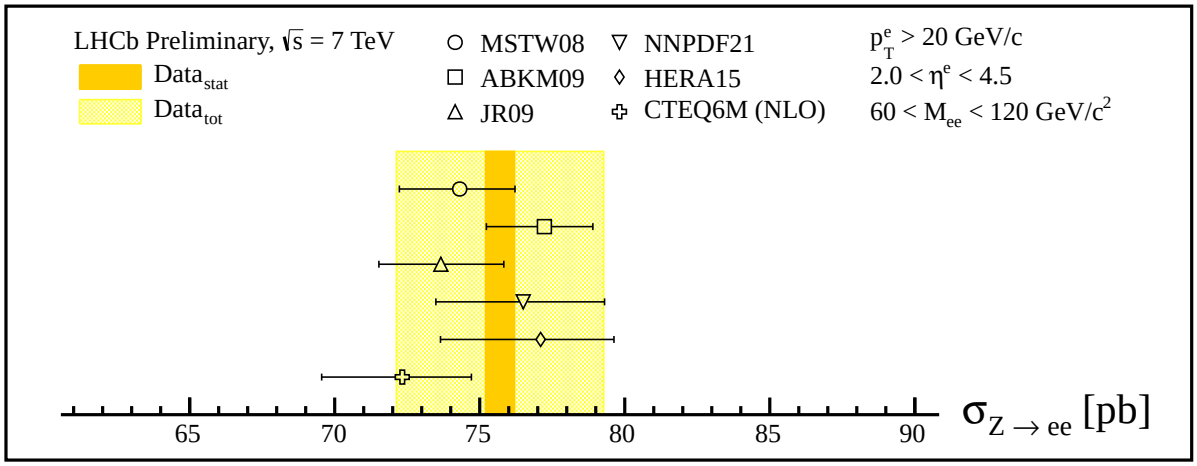

Figure 2: The $Z^0 \to e^+e^-$ production cross-section measured in the 2011 LHCb data, shown as the yellow band. The inner (darker) band represents the statistical error, and the outer the total error. The measurement corresponds to the kinematic acceptance, $p_T > 20$ GeV and $2 < \eta < 4.5$ for the leptons and $60 < M < 120$ GeV and $2 < y < 4$ for the Z^0. The points show the various theoretical predictions described in the text, with errors reflecting their (68% confidence level) uncertainties.

PDF uncertainty, evaluated at the 68% confidence level, and the theoretical uncertainties are added in quadrature to obtain the uncertainties of the predictions.[3] In Fig. 2 we compare the measured cross-section with the six calculations, which all show reasonable compatibility with the data. In Fig. 3 we compare the measurements in the four rapidity bins with the calculations; again the expectations agree with the data within the errors.

[3]The uncertainties for the PDF set CTEQ6M which are given at 90% CL are divided by 1.645.

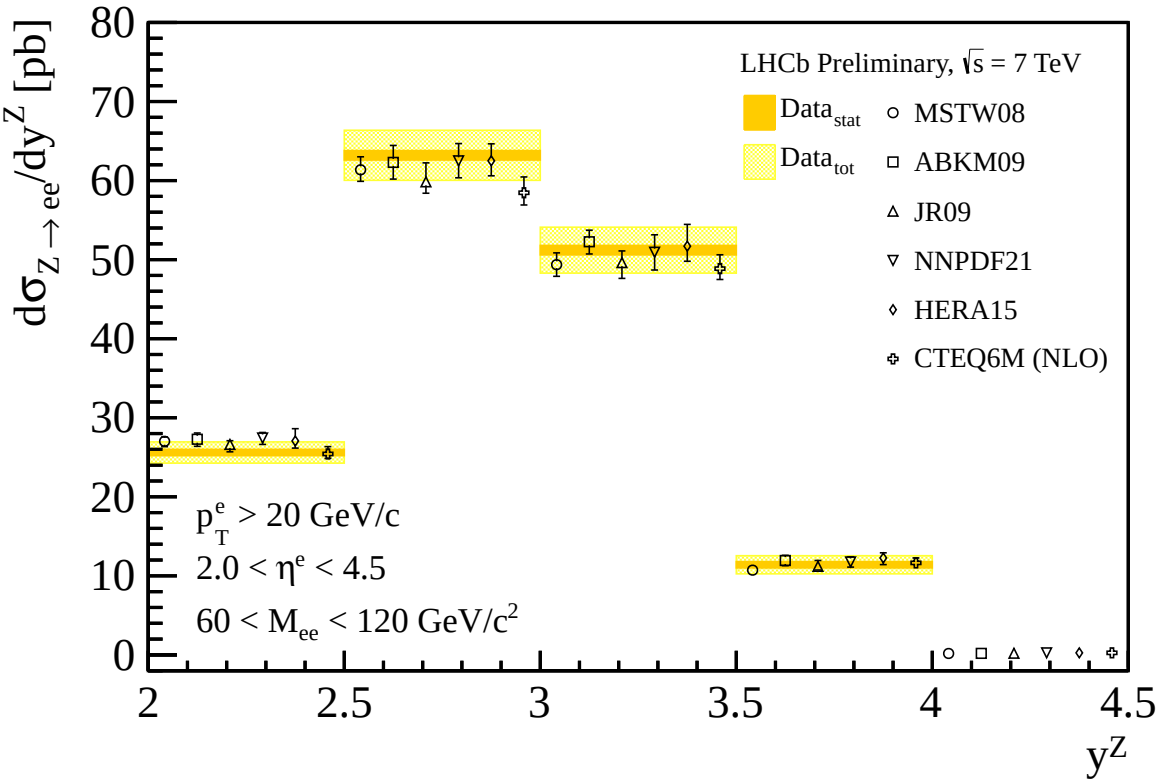

Figure 3: Differential production cross-section for $Z^0 \to e^+e^-$ in bins of Z^0 rapidity. The measurements based on the 2011 LHCb data are shown as the yellow shaded band, where the inner (darker) band represents the statistical error, and the outer the total error. QCD predictions are compared using the points with error bars reflecting their (68% confidence level) uncertainties. These correspond to the same binning as the data, and are displaced sideways in the interest of clarity.

6 Summary

In this note we have presented a measurement of the $Z^0 \to e^+e^-$ cross-section in pp collisions at $\sqrt{s} = 7$ TeV using 945 pb^{-1} of data recorded by LHCb in 2011. The characteristics of the LHCb detector prevent a sharp mass peak from being reconstructed, but despite this a clean sample of events has been identified, with less than 3% background (which is estimated from the data). Within the kinematic acceptance, $p_{\rm T} > 20$ GeV and $2 < \eta < 4.5$ for the leptons and $60 < M < 120$ GeV and $2 < y < 4$ for the Z^0, the cross-section is measured to be

$$\sigma(Z^0 \to e^+e^-) = 75.7 \pm 0.5(\text{stat.}) \pm 2.4(\text{syst.}) \pm 2.6(\text{lumi.}) \text{ pb} \ .$$

The cross-section is also measured in bins of the rapidity of the Z^0. The measurements are consistent with previous measurements using muonic decays of the Z^0 [2, 3] and show good agreement with the expectations from NNLO QCD calculations.

Appendix

We show here two further plots which compare the measurements reported here with existing LHCb results using $Z^0 \to \mu^+\mu^-$ [3] and $Z^0 \to \tau^+\tau^-$ [19] decays, which were based on integrated luminosities of 37.1 pb^{-1} and 248 pb^{-1} respectively. In Fig. 4 we compare the cross-section for $Z^0 \to e^+e^-$ with the other channels in the same acceptance, and in Fig. 5 we compare the rapidity distributions measured using the $Z^0 \to e^+e^-$ and the $Z^0 \to \mu^+\mu^-$ processes. The different measurements are seen to be compatible within their errors.

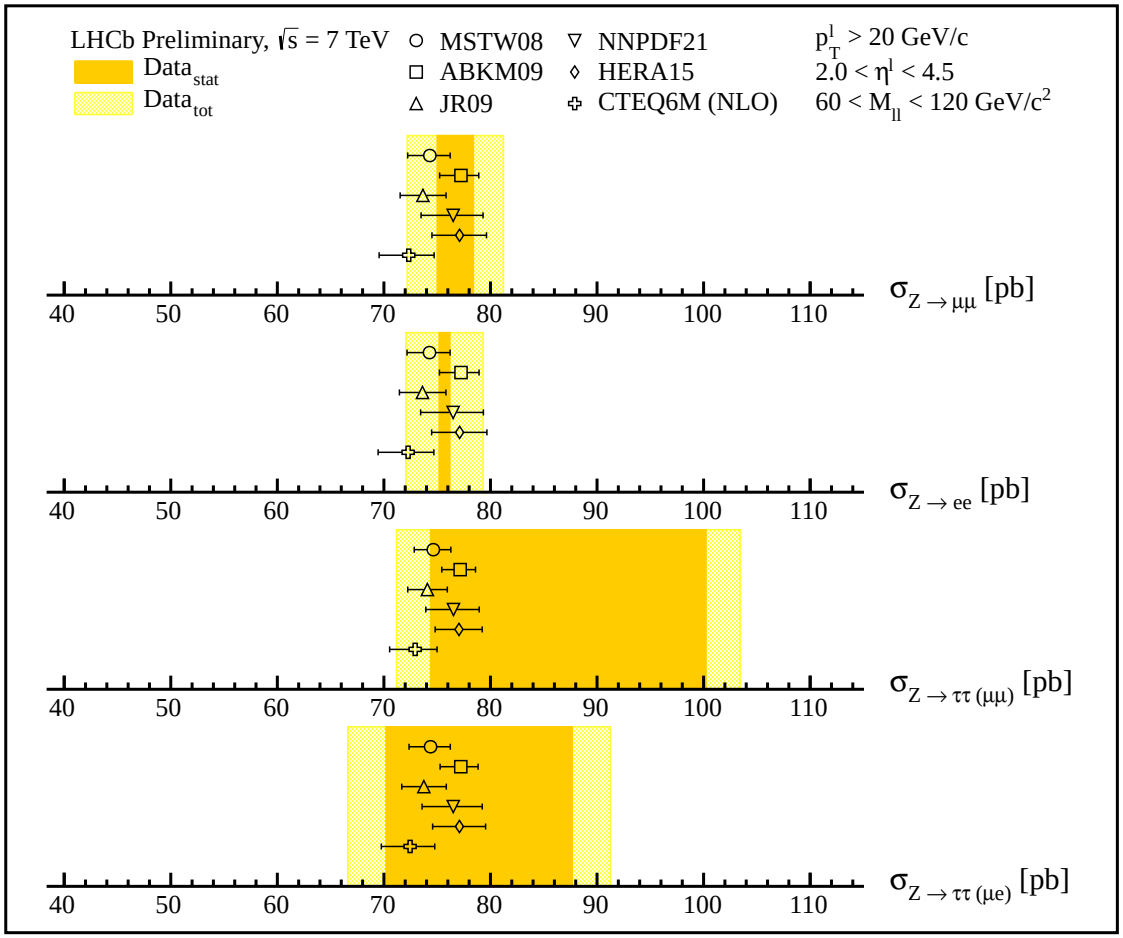

Figure 4: $Z^0 \to \ell^+\ell^-$ production cross-sections, shown as the yellow bands. The inner (darker) bands represents the statistical errors, and the outer the total errors. The measurement corresponds to the kinematic acceptance, $p_T > 20$ GeV and $2 < \eta < 4.5$ for the leptons and $60 < M < 120$ GeV and $2 < y < 4$ for the Z^0. The points show the various theoretical predictions described in the text, with errors reflecting their (68% confidence level) uncertainties.

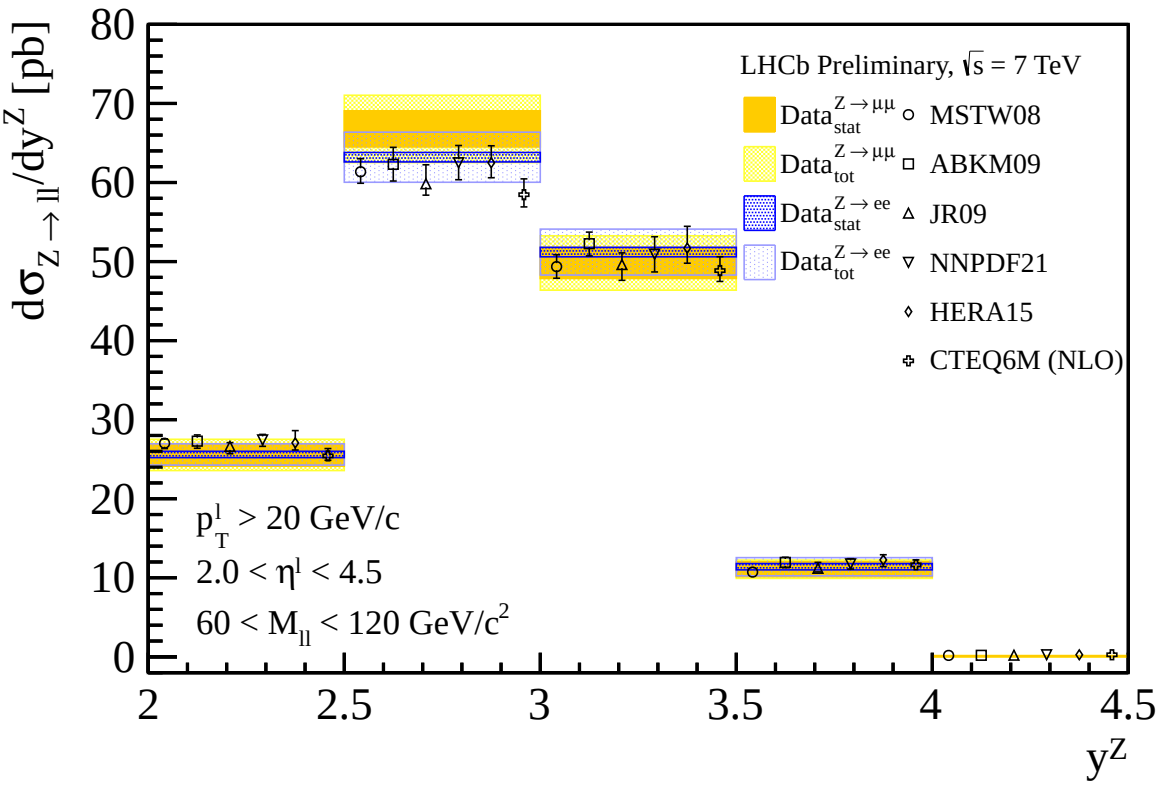

Figure 5: Differential production cross-section for $Z^0 \to \ell^+\ell^-$ in bins of Z^0 rapidity. The measurements based on electrons in the 2011 data are shown as the blue shaded bands and those based on muon data recorded in 2010 are shown as the yellow bands, where the inner (darker) band represents the statistical error, and the outer the total error. QCD predictions are compared using the points with error bars reflecting their (68% confidence level) uncertainties. These correspond to the same binning as the data, and are displaced sideways in the interest of clarity.

References

[1] R. Thorne, A. Martin, W. Stirling, and G. Watt, *Parton distributions and QCD at LHCb*, arXiv:0808.1847.

[2] LHCb collaboration, *Updated measurements of W and Z production at $\sqrt{s} = 7$ TeV with the LHCb experiment*, LHCb-CONF-2011-039.

[3] LHCb collaboration, *Inclusive W and Z production in the forward region at $\sqrt{s} = 7$ TeV*, LHCb-PUB-2012-008.

[4] LHCb collaboration, A. A. Alves Jr. *et al.*, *The LHCb detector at the LHC*, JINST **3** (2008) S08005.

[5] T. Sjöstrand, S. Mrenna, and P. Skands, *PYTHIA 6.4 physics and manual*, JHEP **05** (2006) 026, arXiv:hep-ph/0603175.

[6] I. Belyaev *et al.*, *Handling of the generation of primary events in* Gauss*, the LHCb simulation framework*, Nuclear Science Symposium Conference Record (NSS/MIC) **IEEE** (2010) 1155.

[7] P. M. Nadolsky *et al.*, *Implications of CTEQ global analysis for collider observables*, Phys. Rev. **D78** (2008) 013004, arXiv:0802.0007.

[8] GEANT4 collaboration, S. Agostinelli *et al.*, *GEANT4: A simulation toolkit*, Nucl. Instrum. Meth. **A506** (2003) 250.

[9] M. Clemencic *et al.*, *The LHCb Simulation Application, Gauss: Design, Evolution and Experience*, J. of Phys: Conf. Ser. **331** (2011) 032023.

[10] LHCb Collaboration, R. Aaij *et al.*, *Absolute luminosity measurements with the LHCb detector at the LHC*, JINST **7** (2012) P01010, arXiv:1110.2866.

[11] P. Golonka and Z. Was, *PHOTOS Monte Carlo: a precision tool for QED corrections in Z and W decays*, Eur. Phys. J. **C45** (2006) 97, arXiv:hep-ph/0506026.

[12] C. Carloni Calame, G. Montagna, O. Nicrosini, and A. Vicini, *Precision electroweak calculation of the production of a high transverse-momentum lepton pair at hadron colliders*, JHEP **10** (2007) 109, arXiv:0710.1722.

[13] S. Catani and M. Grazzini, *An NNLO subtraction formalism in hadron collisions and its application to Higgs boson production at the LHC*, Phys. Rev. Lett. **98** (2007) 222002, arXiv:hep-ph/0703012.

[14] A. Martin, W. Stirling, R. Thorne, and G. Watt, *Parton distributions for the LHC*, Eur. Phys. J. **C63** (2009) 189, arXiv:0901.0002.

[15] S. Alekhin, J. Blumlein, S. Klein, and S. Moch, *The 3, 4, and 5-flavor NNLO parton from Deep-Inelastic-Scattering data and at hadron colliders*, Phys. Rev. **D81** (2010) 014032, arXiv:0908.2766.

[16] P. Jimenez-Delgado and E. Reya, *Dynamical NNLO parton distributions*, Phys. Rev. **D79** (2009) 074023, arXiv:0810.4274.

[17] H1 and ZEUS collaborations, F. Aaron *et al.*, *Combined measurement and QCD analysis of the inclusive $e^{\pm}p$ scattering cross sections at HERA*, JHEP **01** (2010) 109, arXiv:0911.0884.

[18] R. D. Ball *et al.*, *A first unbiased global NLO determination of parton distributions and their uncertainties*, Nucl. Phys. **B838** (2010) 136, arXiv:1002.4407.

[19] LHCb collaboration, *Z cross-section measurement at $\sqrt{s} = 7$ TeV using the channel $Z \to \tau\tau$*, LHCb-CONF-2011-041.